Science Arts & Métiers (SAM)

is an open access repository that collects the work of Arts et Métiers Institute of Technology researchers and makes it freely available over the web where possible.

This is an author-deposited version published in: https://sam.ensam.eu
Handle ID: .http://hdl.handle.net/10985/11192

To cite this version :

Alexander NIKITIN, Thierry PALIN-LUC, Andrey SHANYAVSKIY - Fatigue crack initiation and growth on an extruded titanium alloy in gigacycle regime: comparison between tension and torsion loadings - 2016

Any correspondence concerning this service should be sent to the repository Administrator : scienceouverte@ensam.eu

Arts et Métiers Institute of Technology

21st European Conference on Fracture, ECF21, 20-24 June 2016, Catania, Italy

Fatigue crack initiation and growth on an extruded titanium alloy in gigacycle regime: comparison between tension and torsion loadings

Alexander Nikitin[a,b,c]*, Thierry Palin-Luc[c], Andrey Shanyavskiy[d]

[a]*ICAD Russian Academy of Science – 19/18, 2nd Brestskay street, Moscow, Russia*
[b]*MAI – National Research University, 4, Volokolamskoe Hw, Moscow, Russia*
[c]*Arts et Metiers Paris Tech, I2M, CNRS, Esplanade des Arts et Metiers, Talence, France*
[d]*Aviaregister, Air.Sheremetievo-1, PO Box 54, Moscow reg., Chimkovskiy state, Russia*

Abstract

This paper is focused on the analysis of fatigue crack initiation and growth mechanisms in defect free VT3-1 titanium alloy (similar to Ti6Al4V) in VHCF regime under tensile and torsion loadings. Fully reversed fatigue tests were carried out between 10^7 and 10^9 cycles at 20 kHz under constant amplitude loadings (no pulse-pause). SEM observations of the specimens fracture surfaces were carried out in order to compare the crack initiation mechanisms and the different crack growth stages under different loadings. It has been shown that subsurface crack initiation may appear under tension (as usual in gigacycle regime) but in our experiments no inclusion was observed in the "fish-eye". Furthermore, subsurface crack initiation was observed under torsion loading too, despite the maximum shear stress location at the specimen surface. Under this loading, a "fish-eye" was observed too, but again without any inclusion in its center. The suspected microstructural reasons responsible for subsurface crack initiations under torsion loading could not be observed due to significant destruction of the fracture patterns (crack lips friction under mixed mode). The results of the fatigue tests show a principal difference in crack initiation and early crack growth stage between tensile and torsion loadings. Torsion crack initiates on a plane of maximum shear stress (like in HCF regime) while tensile crack is on a plane of maximum normal stress. Sequences of changes in fracture surface roughness is the same for tensile and torsion loadings.

Keywords: compressor disk; titanium alloy; very high cycle fatigue; ultrasonic; torsion; tension; crack initiation mechanism; crack growth;

* Corresponding author. Tel.: +7-965-436-59-80;.
E-mail address: nikitin_alex@bk.ru

1. Introduction

In the last two decades studying the fatigue strength of metals in VHCF regime has become an important scientific subject and then an industrial problem. First, ultrasonic machines that are now commonly used for VHCF tests were capable to carry out tensile tests only, as shown for instance by Neppiras (1959) and Bathias (2005). However, structural elements of real components are subjected to complex multiaxial loadings. In some special cases, such as springs or torque transmission shafts, the cyclic torsion load is more important than the cyclic tension–compression one as reported by Mayer (2006). Therefore, investigating the torsion fatigue strength is a very important industrial problem. The development of ultrasonic torsion testing devices by Stanzl-Tschegg (1993), Bayraktar (2010), Nikitin (2015) has made possible the investigation of the torsion VHCF properties of structural metals.

Xue et al. (2010) have shown interesting scientific results on steels: subsurface crack initiation from elongated inclusions has been observed under torsion loading in spite of the maximum shear stress acting at the specimen surface. The same result was obtained for other metallic materials with strong defects of microstructure. Since the detection of subsurface crack initiation under VHCF torsion loading, an important scientific question has arrived: are the mechanisms of subsurface crack initiation the same or not under tension and torsion loadings? Due to limitation of torsion fatigue data for structural metals there are not many works comparing the mechanisms of subsurface crack initiations. However, there are at least two works: Xue et al. (2010) and Mayer et al. (2006) with VHCF results under tension and torsion on the same material.

According to Xue et al. (2010), for steels, the crack initiation mechanisms are not completely the same under these two types of loading. Furthermore, the chemical composition and geometry of inclusions that lead to subsurface crack initiation are not the same under torsion and under tension loadings. Thus, crack initiation mechanisms should be different. In the case of aluminum alloy, Mayer et al. (2006) outlined also the difference in crack initiation and crack propagation mechanisms. According to these authors, the torsion crack initiates on a plane of maximum shear stress while the crack under tensile loading is on a plane of maximum normal stress. An important conclusion of Mayer (2006) is that crack growth stage under torsion loading is higher compared to the tensile one. The same result was obtained for steels by Bayraktar et al. (2010). The longer crack growth lifetime under torsion loading is explained by the orientation of the crack along the specimen axis and also by an intensive branching of the torsion crack. Such character of torsion crack growth should reduce the effective stress intensity factor range at the crack tip. As it is clear from fracture surface observations done by Shanyvskiy (2007) and Bathias (2010) the roughness of the fracture pattern is depending on the crack growth rate. At the same time, a crack growth rate is linked to the stress intensity factor range and, therefore, the roughness of tensile and torsion fracture patterns could be different.

This paper is focused on comparing fracture surfaces and fatigue test data obtained under tensile and torsion loadings in VHCF regime on VT3-1 titanium alloy.

Nomenclature

UTS – ultimate tensile strength
Y – yield stress
E – Young modulus
E_D – dynamic modulus

2.1 Material

The investigated material is a two-phase (alpha-beta) titanium alloy processed in cylindrical bars of 10 mm in diameter by extrusion technique. The chemical composition of the alloy is the following (w%): 6Al-2Cr-2Mo and Ti balance that is corresponding to VT3-1 titanium alloy according to the Russian classification GOST (2009). The mechanical properties of this extruded VT3-1 titanium alloy were determined on ASTM standard tensile specimens machined from the bars. Tensile tests were performed in laboratory air at room temperature with loading rate 0.0075

mm/min. The results of monotonic quasi-static tensile tests are the following: UTS = 1107 MPa, σ_Y = 1050 MPa, elongation at rupture = 13 %, E=106 GPa and the dynamic modulus at 20 kHz is E_D = 106 GPa. Before any mechanical tests the bars of this titanium alloy were treated in the way that provides a fully lamellar needle-like microstructure, Figure 1. The previous mechanical properties were determined on the treated alloy. Alpha-phase platelets are in white and beta-phase is in black on this figure. The alpha-platelets are elongated in the direction of extrusion and have characteristic length of 2 micrometers. Cross section of these platelets has an almost circular geometry, figure 1a.

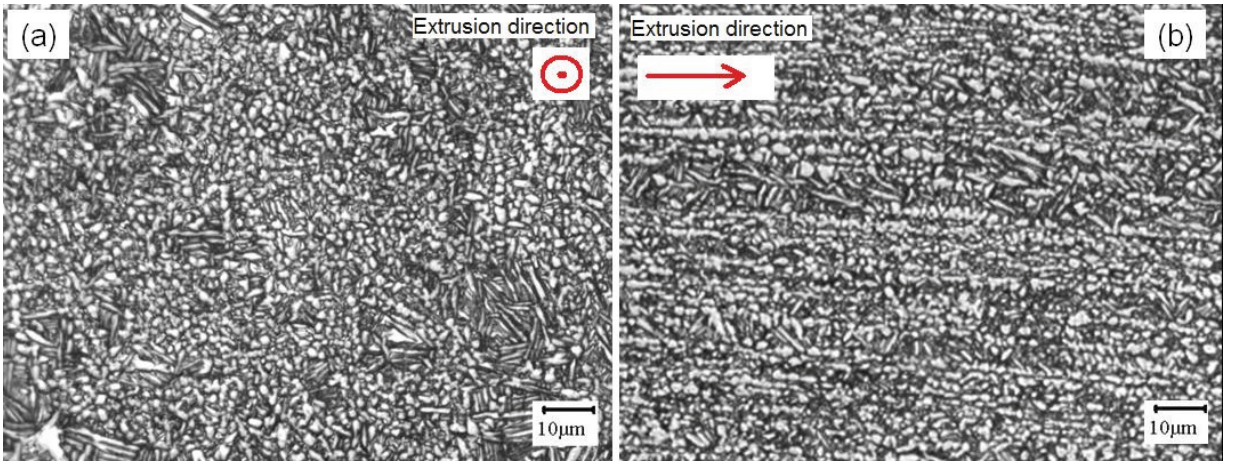

Fig. 1. Microstructure of extruded VT3-1 titanium alloy on planes (a) perpendicular and (b) parallel to extrusion direction.

At some locations the microstructure exhibits very thin alpha-platelets with a length of about 10 micrometers. The microhardness of the extruded VT3-1 titanium alloy was measured by the Vickers method with the following parameters: force 500 N, indentation time: 10 sec. Microhardness values were measured automatically at 15 different locations along a straight line on two planes (perpendicular and parallel to the extrusion direction). The results show almost the same microhardness mean values on the two planes: 374 HV_{500} and 371 HV_{500} on the planes perpendicular and parallel to the extrusion direction respectively. The scatter is very small: the maximum deviation from the mean value is 8 HV_{500}.

1.1. Specimens

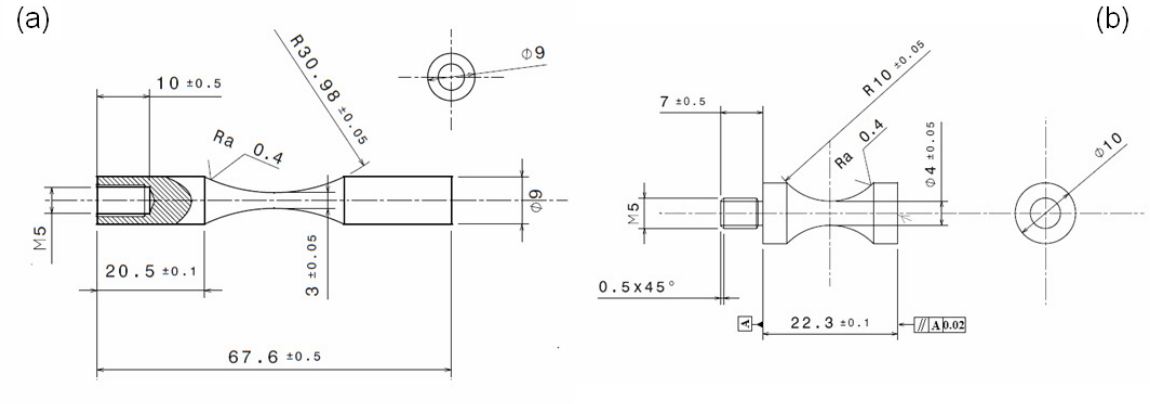

Fig. 2. Geometry of (a) tensile and (b) torsion ultrasonic fatigue specimens in extruded VT3-1 alloy.

Specimens for tensile and torsion fatigue tests were designed according to the ultrasonic concepts detailed in Bathias (2005). The working sections (reduced part) were kept the same and identical to the specimen's geometry usually used in ultrasonic fatigue tests as illustrated in figure 2. The resonance lengths (cylindrical part) were adjusted to get a natural frequency of 20 kHz in tension and torsion modes respectively. All the specimens were machined from the extruded bars by turning. After machining, the median torus of all the specimens was mechanically polished with silicon carbide papers by using grades 600, 800 and 1000.

1.2. Ultrasonic fatigue testing machine and procedure

The principle of the ultrasonic fatigue testing procedure is to excite the specimen at the frequency of one of its natural frequency, Bathias (2005). Under fully reversed tension the excitation has to be the first longitudinal tension-compression mode. Geometries of the loading train components (horn and booster if needed) and specimen are design so that they provide natural frequency of push-pull at 20 kHz. In the case of torsion the same ultrasonic concept is used but instead of axial push-pull mode the first torsion mode has to be used as explained by Bathias (2005) and Nikitin (2015). The two testing systems are controlled by a personal computer with a high-performance feedback.

Fully reversed tension and torsion fatigue tests were carried out under constant amplitude loadings (i.e. continuous regime without pulse-pause). In order to avoid any temperature rise due to self-heating effect the specimen's surface was permanently cooled by compressed dry air passing through an air-gun. For some specimens the surface temperature was measured during ultrasonic fatigue test by using an infrared camera. The results of IR temperature measurements show that the surface temperature in tension and torsion tests was not elevated significantly (i.e. the maximum temperature variation, compared to the room temperature, in our testing conditions is 14 °C). All the tests were performed in laboratory air environment up to the run out limit of 10^9 cycles or specimen failure. Fatigue cracks were detected automatically as natural frequency drop out of the range [19.5 – 20.5 kHz] that is a frequency drop of 2.5 % for a loading frequency of 20 kHz.

2. Results

2.1. SN-curves

The results of ultrasonic tension and torsion fatigue tests are illustrated in Figures 3a and 3b respectively. As already did by Sonsino et al. (1997) in high cycle fatigue, the Von-Mises equivalent stress can be used to assess the torsion fatigue strength from the tension one. That is why the tension and torsion fatigue data are plotted on the same graph by using the Von-Mises equivalent stress (Figure 3). The results of torsion tests in terms of equivalent stresses are presented on figure 3a with diamond symbols and dashed line. One can see that the Von Mises equivalent stress is not suitable to correlate the tension and torsion fatigue strength in the VHCF regime. Furthermore, despite the large scatter of the fatigue data one can see that the slope of the S-N curve in torsion is a little bit higher than in tension. The torsion results re-calculated by using Von-Misses equivalent stresses are placed higher on the S-N curve diagram than the tension results (Figure 3a). This is different from the published data on steels in HCF regime by Sonsino (1997) on steel and even on aluminum alloy in VHCF by Mayer (2006). This outlines that each material could have its own behavior in the VHCF regime depending on its microstructure.

Fracture surfaces analysis of all the specimens has shown that no tension specimen failed by surface crack while some torsion specimens have a surface crack initiation. A very interesting result is that the majority of the cracked torsion specimens have subsurface crack initiation in spite of maximum shear stress location at the specimen surface. Surface crack initiation under torsion loading is common in HCF regime and the scenario of such initiation is practically the same that is in the case of VHCF, as shown by Nikitin (2016). The case of subsurface crack initiation under torsion load is more interesting.

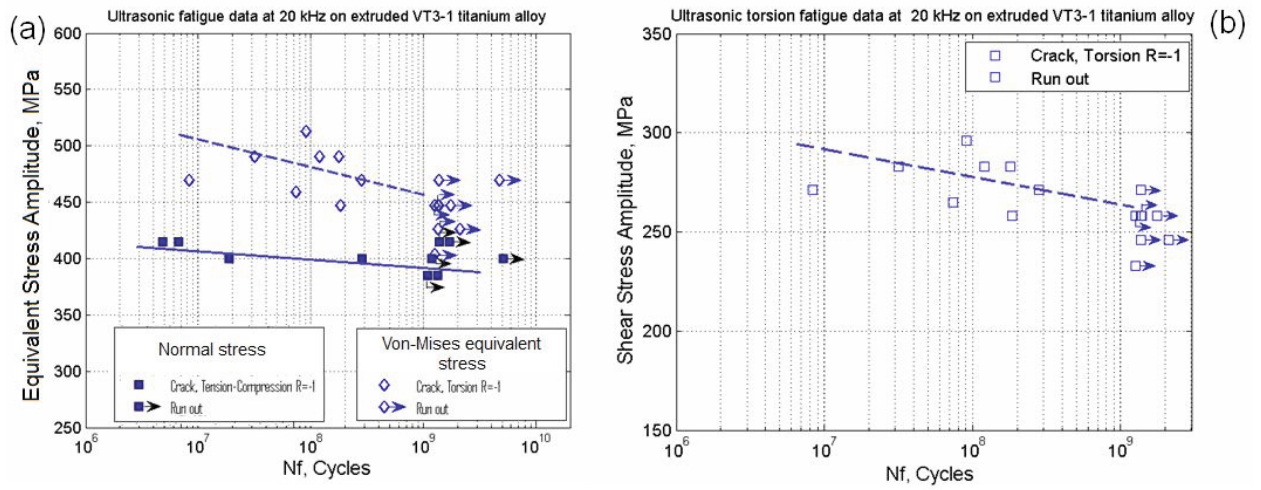

Fig. 3. Results of ultrasonic fatigue tests under fully-reversed tension and torsion plotted in Von Mises equivalent stress amplitude (a) and torsion (b) fatigue tests on extruded VT3-1.

3.2. Fracture surfaces

Typical fracture surfaces with subsurface crack initiation are presented in figure 4 for both tensile and torsion loadings. These patterns are not the same, but in the two cases a very clear 'fish-eye' can be recognized.

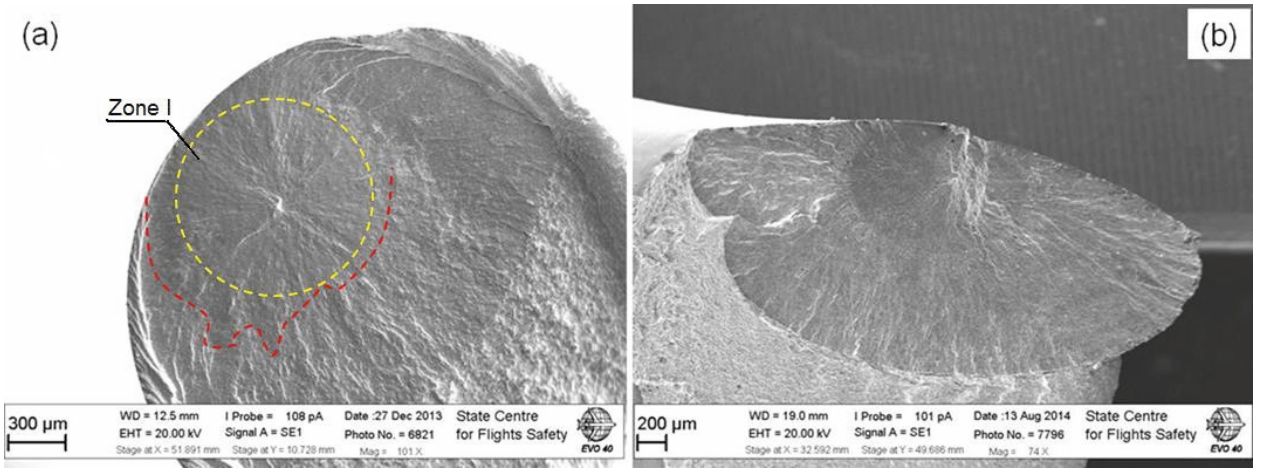

Fig. 4. Fracture surface with subsurface crack initiation and clear 'fish-eye' under (a) tension and (b) torsion fully reversed loadings.

In the case of tension loading (figure 4a) the crack initiation site, early crack growth and long crack growth regime are macroscopically located on the same plane. This is the plane experiencing the maximum normal stress amplitude. The 'fish-eye' has a classical circular shape as observed by Bathias (2005) and Sakai (2009) for example. But, we never observed any inclusion in the center of the fish-eye as it is usually observed in literature (see for instance: Bathias (2005), Sakai (2009), Nishijima (1999)). Internal fatigue crack initiates from a structural inhomogeneity (agglomeration of thin alpha-platelets formed within primary beta-phase) of VT3-1 titanium alloy. The crack initiation site is surrounded by a circular area with lower roughness (zone I on figure 4a). Outside of zone I a color change from dark to light gray can be observed. This transition is outlined by red dashed line. The border of the darker area is not regular and cannot be uniquely determined on the all fracture surface. The transition from dark to light color is related to change in crack growth character. The area with darker color corresponds to subsurface crack growth stage while light gray color is characteristic to the crack appearance at the surface and then its propagation in contact with air.

In the case of torsion crack (figure 4b) the fatigue crack initiation is located on a plane of maximum shear stress (i.e. perpendicular to the picture plane on figure 5). Crack initiation site is significantly destroyed by friction due to crack lips contact because of pure shear cyclic loading. Therefore, the state of the fracture surface does not allow us to identify any microstructural features that are responsible for subsurface crack initiation.

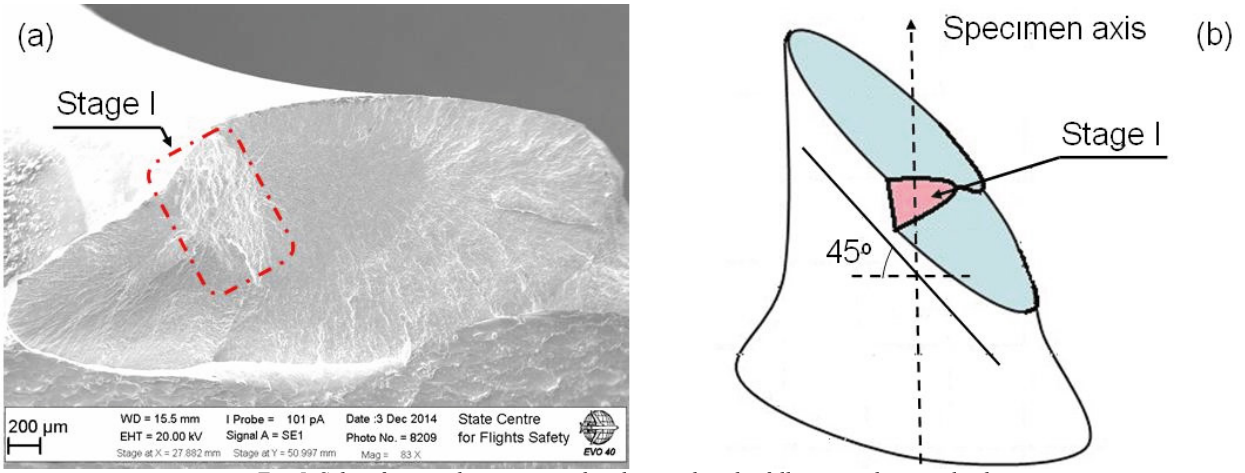

Fig. 5. Subsurface crack initiation and early growth under fully reversed torsion load.

After the crack initiation and early growth on the plane of maximum shear stress amplitude, the torsion crack propagates on a plane experiencing the maximum normal stress amplitude. Like under fully-reversed tension a clear color modification can be observed on the fracture surface, figure 4b. This difference is also related to different crack growth stages. Darker color zone is formed due to subsurface crack growth and light gray color zone is formed due to surface crack growth stage. The border between these two zones is very clear and can be easily determined over the whole fracture pattern. At the end of the subsurface crack growth stage, the shape of the front of the crack is ellipsoidal with an eccentricity not very far from zero. Beyond the subsurface crack growth regime the final crack front has kept an ellipsoidal shape but its eccentricity has increased. The roughness of the fracture surface corresponding to the surface crack growth stage has also increase significantly. Thus, despite the difference at the crack initiation and early crack growth stages, the final fracture patterns under tensile and torsion loads are qualitatively similar.

The fracture surfaces analysis by SEM of all the specimens has shown that no tension specimen failed by surface crack initiation while some torsion specimens had a surface crack initiation. There was always fish-eye on the specimens loaded in tension that is classic in gigacycle regime. But a very interesting result is that the majority of the cracked torsion specimens have a subsurface crack initiation despite the maximum shear stress location at specimen surface. The surface crack initiation under torsion load is common for HCF regime and a scenario of such initiation is practically the same that is in the case of VHCF Nikitin (2016). The case of subsurface crack initiation under torsion load is more interesting.

3. Discussion

As already mentioned, the analysis of the S-N curves, figure 3, shows that the Von-Mises equivalent stress cannot be used to assess the torsion fatigue strength of the extruded titanium alloy in VHCF regime from the tension fatigue data. This result is different from the published data by Sonsino et al. (1997) on steels in HCF regime and on aluminum alloy in VHCF by Mayer et al. (2006). This outlines that each material may have its own behavior in the VHCF regime depending on its own microstructure. Some features of the extruded VT3-1 titanium alloy microstructure (agglomerations of primary beta phase grains filled by thin alpha-platelets) are more sensitive to the tensile loading than to the torsion one. Torsion results re-calculated by using Von-Misses equivalent stresses are placed higher on the SN-curve compared to the tension results. However, the slope of the torsion S-N curve is a little

bit higher, that is probably related to loading mode. In the work Oguma (2010) it was outlined that the fatigue strength of Ti-6Al-4V was permanently decreasing versus the number of cycles under fully reversed tension, but it had a clear step-wise shape in the case of loading with positive stress ratio R=0.1. This means that the fatigue behavior of titanium alloys may have a high sensitivity to the loading mode in VHCF regime. Difference in VHCF strength can be due to the different crack initiation mechanisms activated by the different loading types.

In the case of extruded VT3-1 titanium alloy crack initiation under tension loading is related to agglomerations of thin alpha-platelets, figure 6. These agglomerations are failed in shear mode at the microscopic scale level that can be seen from inclined facet at the origin of the fatigue crack. However, after the initiation in inclined plane the fatigue crack is remaining to the plane experiencing the maximum normal stress. Therefore, the mode II crack growth stage is limited by a few micrometers. In the case of torsion loading crack initiation is also in mode II, however an early crack growth stage can be more significant, figure 5a. The higher sensitivity of VT3-1 titanium alloy to mode II loading may lead to a S-N curve. The crack initiation in mode II under tension load further leads to split cracking (a crack simultaneously developed in two parallel planes).

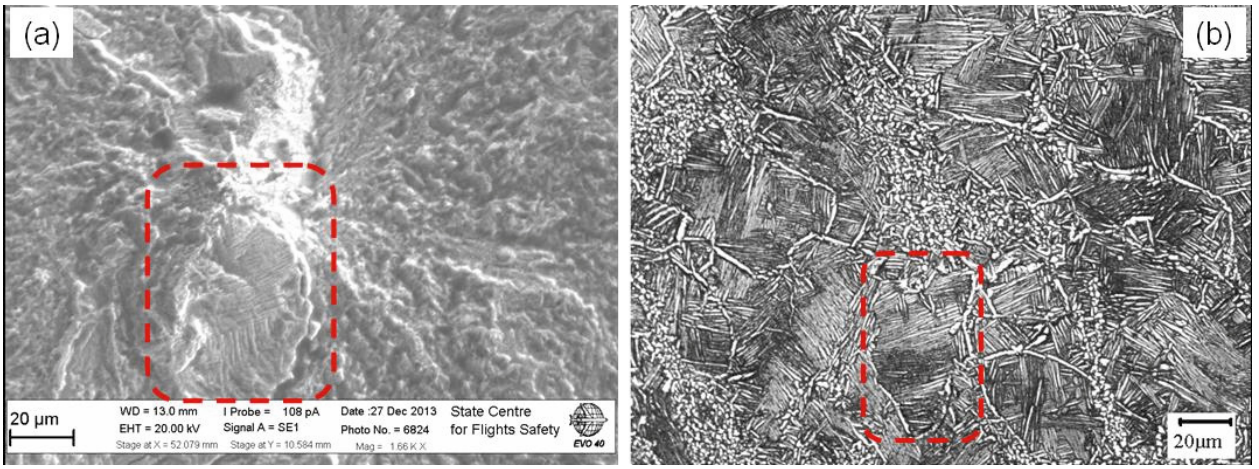

Fig. 6. Crack initiation in extruded VT3-1 titanium alloy from agglomeration of alpha-platelets (a) and corresponding feature of microstructure (b) of extruded VT3-1 alloy.

Fusion of these split cracks lead to form a clear river-like structures starting from the crack initiation, figure 4a. These marks are known also as a 'butterfly wings' in steels. In the case of torsion loading a similar river like structures can be observed, figure 5a, but these features are placed far from the crack initiation site. In the case of torsion load a mechanism of 'wings' structures formation is different from the tension case. After the stage I growth in mode II, figure 5, and the main torsion crack turns to propagate under mode I. During the subsurface stage of torsion crack growth the Mode I cracking dominates over Mode II and Mode III cracking. When the torsion crack reaches the specimen surface the stress state is changing that leads to an increasing of the crack growth rate. This change can be clearly seen from the color change on the fracture surface, figure 4b. The shape of the final torsion crack is changing from near to circular to clear ellipsoidal. At this stage several secondary cracks on alternative planes experiencing the maximum normal stress may start to develop. The coalescence of the main crack with these secondary cracks produces'wings-like' structures on the torsion fracture surface.

Therefore, it seems that fracture surfaces under tension and torsion loads are qualitatively similar. Both fracture surfaces shows a developed 'fish-eye' crack with all usually distinguished zones. However the mechanisms of some elements of the fracture pattern formation are not completely the same for these two loading types. Both tension and torsion cracks are initiated in Mode II, however the duration of early fatigue crack growth under Mode II is not the same for these loadings. Further crack growth stage is being found under Mode I for tension and torsion crack. During this crack growth stage the mechanism of cracking could be the same and the same color change at transition from subsurface to surface crack propagation regime was observed for both loading mode. The final answer to the question about similarity of crack growth mechanisms at this stage can give additional information for calculating the stress intensity factors (SIF) at the border of the transition for the two loading types. Surface crack growth stage

is not the same for tension and torsion loading mode. The difference is that under torsion an active crack branching can be observed while under tension load just one main crack is observed up to the final crack length. Therefore, the conclusion of Bayraktar (2010) about longer crack growth stage for torsion crack is reasonable for VT3-1 titanium alloy too.

4. Conclusion and prospects

Based on the obtained results the following points can be outlined:

(1) Subsurface crack initiations were observed in VHCF regime under fully reversed torsion despite the location of the maximum shear stress amplitude at the specimen surface.

(2) A torsion "fish-eye" was observed both under tension and torsion fully reversed loadings, but in each case no inclusion was observed in the center of the "fish-eye" (as it is usually the case on many steels in VHCF regime).
Because of the friction on the lips of the torsion crack, the microstructural features responsible for the crack initiation could not be identified. Whereas under tension loading, the initiation has been observed on an agglomeration of thin alpha-platelets formed within the primary beta-phase

(3) Crack initiation and early growth under torsion loading is on the plane experiencing the maximum shear stress amplitude, while under tensile loading the crack initiation is on the plane of maximum normal stress. Further crack growth on the plane of maximum normal stress is qualitatively the same for torsion and tensile loadings

(4) Qualitatively the same 'fish-eye' pattern is formed under the two loading types. Sequence of crack growth stages and roughness changes is the same manner for tensile and torsion loading

(5) The stage of subsurface crack growth is almost the same for tensile and torsion loadings, while surface crack growth is significantly longer in the case of torsion loading.

(6) The Von-Mises equivalent stress cannot be used for estimating, from VHCF data under tension, the VHCF strength of extruded VT3-1 titanium alloy under torsion loading.

Additional work is needed to propose a VHCF criterion.

References

Neppiras E.A., 1959. Techniques and equipment for fatigue testing at very high frequencies, Proceedings of the 62nd annual meeting of ASTM, Philadelphia: ASTM, 59, 691 – 710.

Bathias C., Paris P.C., (2005). Gigacycle fatigue in mechanical practice, Dekker, New-York.

Mayer H., (2006), Ultrasonic torsion and tension-compression fatigue testing: measuring principles and investigations on 2024-T351, International Journal of Fatigue 28, 1446 - 1455

Stanzl-Tschegg S.E., Mayer H.R., Tschegg E.K., 1993. High frequency method for torsion fatigue testing, Ultrasonics, 31(4), 275 – 280.

Bayraktar E., Xue H., Ayari F., Bathias C., 2010. Torsional fatigue behaviour and damage mechanisms in the very high cycle regime, Archives of Materials Science and Engineering 43(2), 77 – 86.

Nikitin, A., Palin-Luc, T., Bathias, C., 2015. A new piezoelectric fatigue testing machine in pure torsion for ultrasonic gigacycle fatigue tests: application to forged and extruded titanium alloys, FFEMS, 38(11) 1294 – 1304.

Xue H.Q., Bathias C., 2010. Crack path in torsion loading in very high cycle fatigue regime, Engineering Fracture Mechanics 77, 1866 – 1873.

Shanyavskiy, A.A., 2007. Modeling of metals fatigue cracking. Synergetics in aviation. Monograph, Ufa, Russia, *in Russian*.

Bathias, C., Paris, P.C., 2010. Gigacycle fatigue of metalic aircraft components, International Journal of Fatigue 32, 894 – 897.

Russian State Standard GOST-19807-91, 2009. Titanium and wrought titanium alloys.

Sonsino, C.M., Kaufmann, H., Grubisic, V., 1997. Transferability of material data for the example of a randomly loaded truck stub axle, SAE Tech. paper series, 970708, 1-22.

Nikitin, A., Palin-Luc, T., Shanyavskiy, A., Bathias, C., 2016. Crack path in aeronautical titanium alloy under ultrasonic torsion loading. Fracture and Structural Integrity 35, 213 – 222.

Sakai, T., 2009. Review and prospects for current studies on very high cycle fatigue of metallic materials for machine structural use. Journal of Solid Mechanics and Materials Engineering, 3(3), 425-436.

Nishijima, S., Kanazawa, K., 1999. Stepwise S-N curve and fish-eye failure in gigacycle fatigue, Fatigue and Fracture of Engineering Materials and Structures 22, 601 – 607.